Multi-modality diagnostic assessment in interventional cardiology

Pyxaras, S.

Chapter 6

In-stent fractional flow reserve variations and related optical coherence tomography findings: the FFR-OCT Co-registration Study

This chapter was adapted from:
In-stent fractional flow reserve variations and related optical coherence tomography findings: the FFR-OCT Co-registration Study
Stylianos A. Pyxaras, MD, Tom Adriaenssens, Emanuele Barbato, Giovanni Jacopo Ughi, Luigi Di Serafino, Frederic De Vroey, Gabor Toth, Shengxian Tu, Johan HC Reiber, Jeroen J. Bax, William Wijns
International Journal of Cardiovascular Imaging. 2018,
Volume 34, Issue 4, Pages 495-502

ABSTRACT

Objectives. We sought to assess in-stent variations in fractional flow reserve (FFR) in patients with previous percutaneous coronary intervention (PCI) and to associate any drop in FFR with findings by optical coherence tomography (OCT) imaging.

Background. Suboptimal post-PCI FFR values was previously associated with poor outcomes. It is not known to which extent in-stent pressure loss contributes to reduced FFR.

Methods. In this single-arm observational study, 26 patients who previously underwent PCI with drug-eluting stent or scaffold implantation were enrolled. Motorized FFR pullback during continuous intravenous adenosine infusion and OCT assessments was performed. Post-PCI FFR <0.94 was defined as suboptimal.

Results. At a median of 63 days after PCI (interquartile range: 59 to 64 days), 18 out of 26 patients (72%) had suboptimal FFR. The in-stent drop in FFR was significantly higher in patients with suboptimal FFR vs. patients with optimal FFR (0.08±0.07 vs. vs. 0.01±0.02, p<0.001). Receiver operating characteristic (ROC) curve analysis showed that an in-stent FFR variation of >0.03 was associated with suboptimal FFR. In patients with suboptimal FFR, the OCT analyses revealed higher mean neointimal area (respectively: 1.06±0.80 vs. 0.51±0.23 mm^2; p=0.018) and higher neointimal thickness of covered struts (respectively 0.11±0.07 vs. 0.06±0.01 mm; p=0.021).

Conclusions. Suboptimal FFR values following stent-implantation are mainly caused by significant in-stent pressure loss during hyperemia. This finding is associated to a larger neointimal proliferation.

INTRODUCTION

Ischemia-driven percutaneous coronary intervention (PCI) in patients with stable coronary artery disease has been associated with improved clinical outcome (1-3). Targeting PCI to flow-limiting epicardial vessel stenoses with the use of fractional flow reserve (FFR), in combination with newer generation drug-eluting stents (DES) and optimal medical treatment, enriched by thienopyridinic dual antiplatelet therapy regimen, has significantly improved effectiveness of PCI in this clinical subset (4,5).

We hypothesize that post-PCI functional assessment may contribute to further improvement of procedural results. By definition, normal epicardial vessels have an FFR value of 1.0 throughout their entire length, indicating normal arterial conductance (6,7). Accordingly, PCI of hemodynamically relevant stenoses (i.e. FFR <0.80) aims at normalization of arterial conductance and subsequent restoration of myocardial blood flow. Optimal stent deployment by intracoronary IVUS imaging was previously associated with FFR value $\geq$ 0.94 after PCI (8) and suboptimal stent expansion was shown to cause flow pattern alterations and abnormal coronary conductance (9,10). Of note, many patients after anatomically successful PCI are left with suboptimal final FFR values, translating into worse outcomes (11,12). Thus it becomes essential to understand the mechanisms leading to suboptimal post-PCI FFR values, whether related to procedural technique and/or diffuse coronary atherosclerosis.

Highly detailed intracoronary imaging by means of optical coherence tomography (OCT) allows precise in-vivo visualization of stented coronary segments and quantification of vessel-wall or stent-strut abnormalities (13). Therefore, in the present study we sought to assess in-vivo FFR variations in stented coronary segments and to identify related co-registered morphological abnormalities by OCT.

METHODS

Patient population

Patients with previously implanted DES or bioresorbable vascular scaffolds undergoing elective coronary angiography were prospectively enrolled from 1st August 2011 to 31st October 2012 at the Cardiovascular Research Center Aalst, OLV-Clinic, Aalst, Belgium.

Exclusion criteria were myocardial infarction, hemodynamic instability, renal insufficiency, contraindications to intravenous adenosine administration, and anatomical characteristics such as extreme vessel tortuosity and severe calcification that might prevent the advancement of the OCT catheter.

The study was performed in accordance with the guidelines set by the Declaration of Helsinki (14) and with the local legal requirements. No extramural funding was used to sup-

port the study. The authors wrote the manuscript and are responsible for the completeness and accuracy of data gathering and analysis.

Fractional flow reserve measurement – Motorized pullback

Myocardial FFR was measured using a 0.014-inch miniaturized pressure monitoring guide wire system PressureWire, St. Jude Medical, St. Paul, MN, USA). The wire was introduced through a 6F guiding catheter, calibrated before introduced into the guiding catheter, advanced into the coronary artery, and, after equalization, positioned distal to the stenosis as previously described (6,15). Adenosine was administered to induce maximum hyperemia using intravenous infusion at 140 µg/kg/min. FFR was calculated as the ratio of mean hyperemic distal coronary pressure measured by the pressure wire to mean aortic pressure measured by the guiding catheter (Pd/Pa). Previous pioneering experience by Hanekamp et al. showed that FFR in truly normal coronary arteries equals 0.94 to 1.00 (8); optimum stent deployment according to coronary pressure measurement was then defined by a cut-off value of FFR $\geq$0.94. Accordingly, we define suboptimal FFR <0.94 when the pressure wire was placed 10 mm distally to the distal edge of the previously implanted stent (defined as "distal-vessel FFR") (8). This value reflects the overall epicardial vessel conductance.

For the shake of simplicity we report the following Pd/Pa ratios during maximal hyperemia, defined as follows (from distal to proximal):

- Distal-vessel FFR, defined as the FFR value retrieved with the pressure sensor placed 10 mm distally to the distal edge of the stent
- Distal stent-edge FFR, defined as the FFR value retrieved with the pressure sensor placed exactly at the distal edge of the stent
- Proximal stent-edge FFR, defined as the FFR value retrieved with the pressure sensor placed exactly at the proximal edge of the stent
- Proximal-vessel FFR, defined as the FFR value retrieved with the pressure sensor placed 10 mm proximally to the proximal edge of the stent

Accordingly, in-stent gradient was defined as follows:

In-stent gradient = Proximal stent-edge FFR – Distal stent-edge FFR

Motorized pullback of the pressure wire was performed using a conventional pullback-device as previously described (16,17). The pullback was performed under constant maximal hyperemia at speed 1.0 mm/s until the pressure sensor placed at the proximal radio-opaque extremity of the wire tip reached the left main stem or right coronary ostium. Angiography at the initial position of the pressure wire allowed precise localization of the pressure sensor. In case the FFR value in the guiding catheter was not back to 1.00, the pullback was repeated after repeat signal equalization. Digital FFR data were extracted, co-registered with angio-

graphic and OCT data and analyzed off-line using the QAngioOCT Software (QAngioOCT Research Edition 1.0, Medis Specials BV, Leiden, the Netherlands).

Optical coherence tomography – Acquisition and analysis

OCT pullbacks were performed at 20 mm/s by non-occlusive flushing technique using a 2.7 F imaging catheter with a dedicated workstation (C7-XRTM OCT Intravascular Imaging System, St. Jude Medical, St. Paul, MN, USA). Blood was cleared during the pullback by injection of contrast medium at 3-4 ml/sec over a period of 3-4 sec. OCT images were recorded at 100 frames/sec and converted to DICOM format at a resolution of 512 × 512 pixels. Z-offset calibration was performed before converting to DICOM format for the subsequent analysis.

Off-line stent strut analysis was performed using the ODIERNA software (UZ Leuven, Leuven, Belgium). Correspondence of segments between coronary angiography, FFR and OCT was established using QAngioOCT (Research Edition 1.0, Medis Specials BV, Leiden, the Netherlands). Quantitative strut level analysis was performed every third frame (0.6 mm interval) along the entire target segment. Malapposition was identified when the stent lumen distance was greater than the sum of strut thickness plus abluminal polymer thickness, according to each stent manufacturer's specifications, plus a compensation factor of 20 μm to correct for strut blooming, and was considered significant if the stent lumen distance was greater than 200 μm (18-20). The thickness of neointimal hyperplasia was measured as the distance between the luminal surface of the neointima and the adluminal surface of the strut, and an uncovered strut was defined as having a neointimal thickness of 0 mm (21). The percentage of uncovered struts was calculated as (number of uncovered struts/ total number of struts) × 100. A completely covered stent was defined as a stent with all analyzable struts covered by neointima. A cross-section with uncovered struts was defined if ≥ 1 stent struts was uncovered, and a cross-section with uncovered strut ratio >0.3 was defined when the ratio of uncovered struts to total stent struts per cross-section was >0.3 (22). In case of bioresorbable scaffold implantation, strut malapposition (SM) was defined as incomplete scaffold apposition (ISA) area delineated by the abluminal side of the frame border of the malapposed strut (covered or uncovered) and the endoluminal contour of the vessel wall; likewise, Neointimal hyperplasia area was defined as previously reported (Scaffold area –[Lumen area + Black box area]) if all struts were apposed, while it was calculated as ([Scaffold area +ISA area + Malapposed strut with surrounding tissues] – [Lumen area + strut area]) in case of malapposed struts (23).

Statistical analysis

Continuous variables are presented as mean ± standard deviation and were compared using the Student's unpaired t-test for comparisons. Kolmogorov-Smirnov goodness-of-fit test confirmed the normal distribution of the variables reported as mean ± standard deviation. Categorical variables are presented as counts and percentages, and were compared

using chi-square or Fisher's exact tests, as appropriate. All probability values reported are two-sided, and a probability value <0.05 was considered significant. Findings are compared between patient subgroups with suboptimal (FFR <0.94) vs optimal FFR, as assessed at 10 mm distance from the distal edge of the previously implanted stent (defined as "distal-vessel FFR"). The Jonckheere-Terpstra test was used to determine if there is a statistically significant monotonic trend between (sub-)optimal post-PCI FFR and in-stent pressure drop. Receiver operating characteristic (ROC) curve analysis was performed to establish the value of in-stent FFR-drop most predictive for suboptimal FFR. All statistical analyses were performed using SPSS 17.0 (SPSS Inc., Chicago, Illinois).

RESULTS

Patient population

Follow-up invasive diagnostic assessment was performed at a median of 63 days (interquartile range 59 to 64 days) after PCI.

Baseline demographic and clinical characteristics, as shown in **Table 1**, were not different between the two patient subgroups (sub-optimal vs. optimal FFR). Most of the patients (n=21, 80.7%) underwent control coronary angiography with OCT-imaging as part of clinical study protocol following PCI. Of the remaining 5 patients, 3 had evidence of silent ischemia and 2 had recurrent angina. Different DES had been implanted in these patients (**Table 1**). In 2 cases, everolimus-eluting bioresorbable scaffolds were implanted.

Optical coherence tomography results

Cross-section and strut-level OCT analyses are shown in **Table 2**.

Overall, 11,582 stent struts have been analyzed for a total of 919 OCT cross-sections.

By cross-section analysis, mean neointimal area was 0.51±0.23 mm^2 in optimal vs. 1.06±0.80 mm^2 in the suboptimal PCI subgroup (p=0.018). The maximum length of segments with malapposed struts and maximum malapposition distance tended to be larger in patients with suboptimal FFR (respectively: 0.02±0.02 mm vs. 0.07±0.15 mm, p=0.062; and 0.04±0.16 vs. 0.08±0.19 mm, p=0.083).

At the strut-level analysis, neointimal thickness of covered struts was 0.06±0.01 in optimal vs. 0.11±0.07 mm in the suboptimal subgroup (p=0.021).

Fractional flow reserve measurements

The motorized pullback at a speed of 1.0 mm/s, alongside with the co-registration software, allowed the precise localization of every FFR value to the corresponding vessel cross-section (stented or not) (**Figures 1 and 2).** Retrieved FFR values during pullback increased significantly from the distal stent edge to the proximal stent edge in both patients with optimal

Table 1. Baseline demographic, clinical and device-related characteristics of the study population.

	Total (n = 26)	Sub-optimal FFR (n = 18)	Optimal FFR (n = 8)	p
Age (years)	57 ± 18	60.4 ± 12.3	63.7 ± 9.4	0.504
Male, n (%)	20 (76.9)	14 (77.8)	6 (75.0)	0.518
Hypertension, n (%)	14 (53.8)	11 (61.1)	3 (37.5)	0.665
Diabetes, n (%)	2 (7.7)	2 (11.1)	0 (0)	0.372
Hyperlipidemia, n (%)	17 (65.4)	12 (66.6)	5 (62.5)	0.694
Smoker, n (%)	11 (42.3)	8 (44.4)	3 (37.5)	0.973
Family history, n (%)	3 (11.5)	2 (11.1)	0 (0)	0.372
Prior MI, n (%)	13 (50.0)	9 (50.0)	4 (50.0)	0.658
Multivessel disease, n (%)	13 (50.0)	9 (50.0)	4 (50.0)	0.658
Clinical presentation				0.589
• Study-driven control*, n (%)	21 (80.7)	15 (83.3)	6 (75.0)	
• Silent ischemia, n (%)	3 (11.5)	2 (11.1)	1 (12.5)	
• Stable angina, n (%)	2 (7.8)	1 (5.6)	1 (12.5)	
LVEF (%)	67.4 ± 9.6	68.9 ± 9.8	63.9 ± 8.8	0.242
Vessel location				0.117
• LAD	13 (50.0)	12 (46.2)	1 (3.8)	
• Cx	7 (26.9)	4 (15.4)	3 (11.5)	
• RCA	6 (23.1)	3 (11.5)	3 (11.5)	
Diameter Stenosis (%)	20.8 ± 9	20.8 ± 8	20.8 ± 11	0.995
Minimal luminal diameter (mm)	2.37 ± 0.6	2.26 ± 0.5	2.68 ± 0.7	0.095
Reference vessel diameter (mm)	2.98 ± 0.6	2.86 ± 0.6	3.35 ± 0.6	0.061
Number of implanted stents	1.11 ± 0.32	1.05 ± 0.23	1.29 ± 0.49	0.264
Total stent length, mm	23.56 ± 7.37	22.74 ± 5.39	26.57 ± 11.40	0.421
Stent diameter, mm	3.25 ± 0.33	3.21 ± 0.30	3.39 ± 0.41	0.307
Stent type, n (%)				0.245
• BVS	2 (7.8)	1 (5.6)	1 (12.5)	
• Combo	5 (19.2)	4 (22.2)	1 (12.5)	
• EES	10 (38.5)	5 (27.8)	5 (62.5)	
• MICELL	4 (15.4)	4 (22.2)	0 (0)	
• ZES	5 (19.2)	3 (16.7)	2 (25.0)	
• Terumo TCDT	2 (7.8)	2 (11.1)	0 (0)	

Numbers are % (count/sample size) or mean ± SD (N). BVS: bioresorbable vascular scaffold; LVEF: left ventricular ejection fraction; MI: myocardial infarction.

* Study-driven controls were asymptomatic during the index procedure.

functional results (ANOVA p=0.003) and in patients with suboptimal FFR (ANOVA p<0.001). The median in-stent pressure drop was 0.01 for patients with optimal post-PCI FFR and 0.05 for patients with suboptimal post-PCI FFR, respectively. The observed increase in FFR value

Table 2. OCT cross-section and strut-level analyses.

	Suboptimal FFR (n=18)	Optimal FFR (n=8)	p
Cross-section level analysis			
Analyzed cross-sections/patient, n	36±10	34±14	0.654
Struts analyzed/cross-section, n	10.93±2.31	11.46±2.62	0.643
Frequency of cross-sections with uncovered struts, %	30.46±34.96	42.16±24.50	0.354
Frequency of cross-sections with 30% uncovered struts, %	16.8±13.4	13.3±7.7	0.570
Maximum length of segments with uncovered struts, mm	0.72±0.74	0.97±0.70	0.436
Maximum length of segments with malapposed struts, mm	0.07±0.15	0.02±0.02	0.062
Maximum malapposition distance, mm	0.08±0.19	0.04±0.16	0.083
Area of malapposition, mm^2	0.09±0.30	0.08±0.21	0.195
Minimum stent area, mm^2	6.75±2.15	7.48±4.00	0.685
Mean stent area, mm^2	7.64±2.05	8.57±3.62	0.574
Mean neointimal area, mm^2	1.06±0.80	0.51±0.23	0.018
Strut-level analysis			
Number of struts analyzed/patient	407±153	405±246	0.989
Number of uncovered struts/patient	109.47±124.90	113.29±65.92	0.921
Frequency of uncovered struts/patient, %	26.78±30.69	27.97±16.27	0.323
Number of malapposed struts/patient	8.79±16.19	17.86±23.27	0.369
Frequency of malapposed struts/patient, %	2.04±4.49	7.95±13.29	0.290
Neointimal thickness of covered struts, mm	0.11±0.07	0.06±0.01	0.021

Numbers are % (count/sample size) or mean ± SD (N). BVS: bioresorbable vascular scaffold; CABG: coronary artery bypass grafting; CAD: coronary artery disease; LVEF: left ventricular ejection fraction; MI: myocardial infarction; PCI: percutaneous coronary intervention.

from the distal to the proximal edge of the stent was statistically significant (p=0.004). In these latter, the in-stent gradient was significantly higher vs. patients with optimal FFR (0.08 ± 0.07 vs 0.01 ± 0.02, p<0.001). By ROC curve analysis, an in-stent gradient >0.03 was associated with suboptimal FFR (specificity 57%, sensitivity 56%) (**Figure 3**).

DISCUSSION

Main findings of the present study are as follows:

1. We provide a quantification of the in-stent pressure drop, demonstrating that most of pressure drop occurs within the previously implanted stent **(Table 3)**.
2. We find that this in-stent pressure drop is significantly higher in patients that have sub-optimal FFR at follow-up (0.08±0.07 vs. 0.01±0.02, p<0.001) **(Table 3)**.

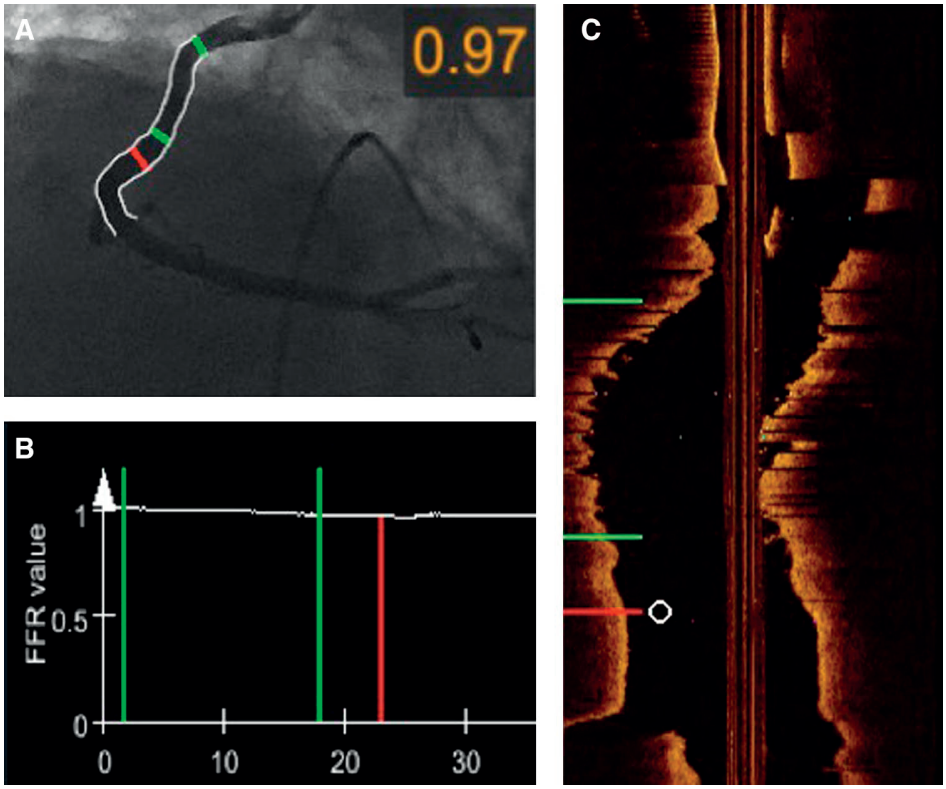

Figure 1. Patient example – Optimal FFR.
Panel A: Coronary angiography of the stented proximal RCA. Panel B: Motorized pullback FFR output, illustrating co-registered FFR values along the distance from distal stent edge till the tip of guiding catheter. Panel C: longitudinal OCT view, showing the strut shadowing.
In each panel, the two green lines correspond to the stent edges, while the red line illustrates the pressure sensor location, as it moved along the analyzed segment. FFR at the present location 5 mm beyond the distal stent edge (red line) was 0.97.
FFR: fractional flow reserve; OCT: optical coherence tomography; RCA: right coronary artery.

3. The OCT strut-level analysis offers an interesting insight of the possible mechanism behind the observed in-stent pressure drop, namely accentuated neointimal hyperplasia, often considered as normal vessel "healing" after stent implant. **(Table 2)**.

This study shows that a sizeable proportion of patients undergoing PCI have sub-optimal FFR values, despite the axiom that stenting of an epicardial stenosis should – theoretically – "normalize" the vessel's conductance. This finding has been previously attributed – at least partially – to diffuse atherosclerotic disease (24,25). Using motorized FFR pullback during hyperemia, co-registered with multiplanar angiography and OCT, we have observed that significant losses in FFR can occur inside previously implanted stents. Using OCT imaging, suboptimal FFR was significantly associated with larger neointimal thickness and area, and

Table 3. Functional measurement during motorized pullback#.

FFR value retrieved by the pressure sensor	Suboptimal FFR (n = 18)	Optimal FFR (n = 8)	p
Proximal-vessel	0.95 ± 0.04	0.99 ± 0.02	0.001
Proximal stent-edge	0.95 ± 0.04	0.98 ± 0.02	0.012
Distal stent-edge	0.87 ± 0.06	0.97 ± 0.02	<0.001
Distal-vessel	0.84 ± 0.07	0.96 ± 0.02	<0.001
p	<0.001	0.003	-
In-stent gradient	0.08 ± 0.07	0.01 ± 0.02	<0.001

Numbers are mean ± SD (N). FFR: fractional flow reserve.
All values are measured – by definition – during maximal hyperemia

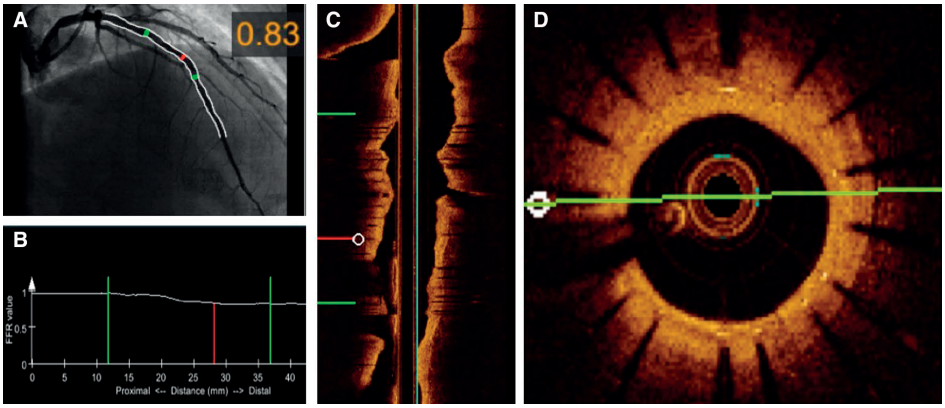

Figure 2. Patient example – Sub-optimal FFR.
Panel A: Coronary angiography of stented mid LAD. Panel B: Motorized pullback FFR output, illustrating co-registered FFR values along the distance from distal stent edge till the tip of guiding catheter. Panel C: longitudinal OCT view, showing the strut artefacts. Panel D: OCT cross-section showing neointimal hyperplasia.
In panel A-C, the two green lines correspond to the stent edges, while the red line illustrates the pressure sensor location, as it moved along the analysis segment. FFR at the present location inside the stent (red line) was 0.83.
FFR: fractional flow reserve; LAD: left anterior descending artery; OCT: optical coherence tomography.

to a lesser extent (trend) with increased length of malapposed struts. Thus, neointimal proliferation following stent implantation, even in the absence of restenosis, may jeopardize the restoration of normal coronary conductance.

Previous studies of putative mechanisms behind in-stent pressure losses were based on intravascular ultrasound (IVUS) imaging studies performed immediately after stent implantation (8,10,26). Insufficient deployment pressure was identified as the principal cause of suboptimal post-PCI FFR, due to gross malapposition visualized by IVUS. Currently, OCT allows qualitative and quantitative assessment of stented coronary segments with unprecedented detail. Using co-registered OCT imaging, we have identified neointimal proliferation as root cause for in-stent pressure loss during hyperemia. In contrast to previous reports, we did not obtain intravascular imaging and FFR measurements immediately after stent implantation,

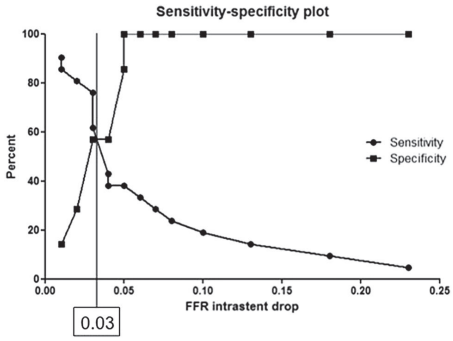

Figure 3. ROC curve analysis to establish the value of FFR drop that is most predictive for suboptimal FFR.
FFR: fractional flow reserve; ROC: receiving operator characteristic.

but during follow-up. Therefore, our findings reflect the anatomical and functional consequences of stent implantation in atherosclerotic epicardial vessels. Other than the pressure-drop observed previously immediately after the stent implantation, we report for the first time a correlation between the neointimal coverage of the implanted stent and sub-optimal FFR-values during follow-up

Neointimal proliferation observed at follow-up can be part of the "healing" mechanism following an initial strut malapposition. Kawamori et al. showed a significant association between the mean neointimal thickness and the OCT-phenotype defined as "resolved malapposed struts" (i.e. malapposition observed immediately after PCI that vanishes at follow-up due to strut coverage from neointima) (27). In addition to these findings, our results suggest that neointimal proliferation at follow-up is a possible cause of in-stent pressure drop, highlighting an active interrelationship of anatomic and functional variations following stent implantation. We observed 4 patients with late stent malapposition (15.4%), similar to the rate observed by Kawamori et al. (17.5%). Despite these relatively small rates, our findings suggest that late stent malapposition may have a role (observed trend) in defining a functionally suboptimal PCI result, which may be part of an abnormal healing process.

Clinical relevance of these findings resonates with prior studies showing that suboptimal FFR after PCI was an independent predictor of adverse events (11,12). In the present study, co-registration with OCT confirms that FFR drop can occur not only outside, but also within the boundaries of the stented coronary segment. On average, 50% of the obstacle to hyperemic flow was located within the stent (**Table 3**), meaning that the loss of in-stent conductance is mainly responsible for the observed drop in FFR value. This mechanism lends itself to improvement through optimization of procedural technique and perfection of stent performance.

Study limitations

Our study is limited by the low patient number, although 10,000+ stent struts and nearly 1,000 cross-sections have been analyzed qualitatively and quantitatively. The observed changes by cross-section and strut-level analyses are unlikely to be associated to clinical events, even with larger sample sizes. Likewise, this was the reason that other possible causes possibly associated with suboptimal PCI results (e.g. plaque protrusion or incomplete stent expansion) were not detected. Second, for the shake of simplicity we report the retrieved Pd/Pa values during maximal hyperemia as FFR values spatially corresponding in different points of the epicardial vessel. We acknowledge that the FFR value, as by definition, is only one for every epicardial vessel (stented or not), expressing the overall vessel conductance. Accordingly, the FFR value corresponds to the hereby reported as distal-vessel FFR (**Table 3**). Third, OCT and FFR measurements were not obtained immediately after stent implantation. Therefore, the dynamics of strut malapposition and coverage as well as their interaction with FFR is unknown. Finally, despite the significant association between in-stent gradient and sub-optimal FFR, sensibility and specificity values were relatively low. Further multi-modality co-registration studies including baseline and follow-up will be needed to elucidate the procedural and biological mechanisms leading to suboptimal FFR values at any point in time.

CONCLUSION

This study demonstrates in vivo that suboptimal FFR values 2 months after PCI are mainly caused by significant in-stent pressure losses that are associated with a larger neointimal proliferation.

REFERENCES

1. Shaw LJ, Berman DS, Maron DJ et al. Optimal medical therapy with or without percutaneous coronary intervention to reduce ischemic burden: results from the Clinical Outcomes Utilizing Revascularization and Aggressive Drug Evaluation (COURAGE) trial nuclear substudy. Circulation 2008;117:1283-91.
2. Tonino PA, De Bruyne B, Pijls NH et al. Fractional flow reserve versus angiography for guiding percutaneous coronary intervention. N Engl J Med 2009;360:213-24.
3. De Bruyne B, Pijls NH, Kalesan B et al. Fractional flow reserve-guided PCI versus medical therapy in stable coronary disease. N Engl J Med 2012;367:991-1001.
4. Bangalore S, Kumar S, Fusaro M et al. Short- and long-term outcomes with drug-eluting and bare-metal coronary stents: a mixed-treatment comparison analysis of 117 762 patient-years of follow-up from randomized trials. Circulation 2012;125:2873-91.
5. Palmerini T, Biondi-Zoccai G, Della Riva D et al. Stent thrombosis with drug-eluting and bare-metal stents: evidence from a comprehensive network meta-analysis. Lancet 2012;379:1393-402.
6. Pijls NH, De Bruyne B, Peels K et al. Measurement of fractional flow reserve to assess the functional severity of coronary-artery stenoses. N Engl J Med 1996;334:1703-8.
7. Pijls NH, Van Gelder B, Van der Voort P et al. Fractional flow reserve. A useful index to evaluate the influence of an epicardial coronary stenosis on myocardial blood flow. Circulation 1995;92:3183-93.
8. Hanekamp CE, Koolen JJ, Pijls NH, Michels HR, Bonnier HJ. Comparison of quantitative coronary angiography, intravascular ultrasound, and coronary pressure measurement to assess optimum stent deployment. Circulation 1999;99:1015-21.
9. Foin N, Gutierrez-Chico JL, Nakatani S et al. Incomplete stent apposition causes high shear flow disturbances and delay in neointimal coverage as a function of strut to wall detachment distance: implications for the management of incomplete stent apposition. Circ Cardiovasc Interv 2014;7:180-9.
10. Matthys K, Carlier S, Segers P et al. In vitro study of FFR, QCA, and IVUS for the assessment of optimal stent deployment. Catheter Cardiovasc Interv 2001;54:363-75.
11. Pijls NH, Klauss V, Siebert U et al. Coronary pressure measurement after stenting predicts adverse events at follow-up: a multicenter registry. Circulation 2002;105:2950-4.
12. Johnson NP, Toth GG, Lai D et al. Prognostic value of fractional flow reserve: linking physiologic severity to clinical outcomes. J Am Coll Cardiol 2014;64:1641-54.
13. Prati F, Regar E, Mintz GS et al. Expert review document on methodology, terminology, and clinical applications of optical coherence tomography: physical principles, methodology of image acquisition, and clinical application for assessment of coronary arteries and atherosclerosis. Eur Heart J 2010;31:401-15.
14. Rickham PP. Human Experimentation. Code of Ethics of the World Medical Association. Declaration of Helsinki. Br Med J 1964;2:177.
15. Bartunek J, Sys SU, Heyndrickx GR, Pijls NH, De Bruyne B. Quantitative coronary angiography in predicting functional significance of stenoses in an unselected patient cohort. J Am Coll Cardiol 1995;26:328-34.
16. Pyxaras SA, Tu S, Barbato E, Reiber JH, Wijns W. Optimization of Tryton dedicated coronary bifurcation system with coregistration of optical coherence tomography and fractional flow reserve. JACC Cardiovasc Interv 2013;6:e39-40.

17. Pyxaras SA, Tu S, Barbato E, Wyffels E, Reiber JH, Wijns W. Co-registration of fractional flow reserve and optical coherence tomography with the use of a three-dimensional angiographic roadmap: an opportunity for optimisation of complex percutaneous coronary interventions. EuroIntervention 2013;9:889.
18. Imola F, Mallus MT, Ramazzotti V et al. Safety and feasibility of frequency domain optical coherence tomography to guide decision making in percutaneous coronary intervention. EuroIntervention 2010;6:575-81.
19. Tanigawa J, Barlis P, Di Mario C. Intravascular optical coherence tomography: optimisation of image acquisition and quantitative assessment of stent strut apposition. EuroIntervention 2007;3:128-36.
20. Prati F, Romagnoli E, Burzotta F et al. Clinical Impact of OCT Findings During PCI: The CLI-OPCI II Study. JACC Cardiovasc Imaging 2015;8:1297-305.
21. Tearney GJ, Regar E, Akasaka T et al. Consensus standards for acquisition, measurement, and reporting of intravascular optical coherence tomography studies: a report from the International Working Group for Intravascular Optical Coherence Tomography Standardization and Validation. J Am Coll Cardiol 2012;59:1058-72.
22. Finn AV, Joner M, Nakazawa G et al. Pathological correlates of late drug-eluting stent thrombosis: strut coverage as a marker of endothelialization. Circulation 2007;115:2435-41.
23. Serruys PW, Onuma Y, Ormiston JA et al. Evaluation of the second generation of a bioresorbable everolimus drug-eluting vascular scaffold for treatment of de novo coronary artery stenosis: six-month clinical and imaging outcomes. Circulation 2010;122:2301-12.
24. Rodes-Cabau J, Gutierrez M, Courtis J et al. Importance of diffuse atherosclerosis in the functional evaluation of coronary stenosis in the proximal-mid segment of a coronary artery by myocardial fractional flow reserve measurements. Am J Cardiol 2011;108:483-90.
25. De Bruyne B, Hersbach F, Pijls NH et al. Abnormal epicardial coronary resistance in patients with diffuse atherosclerosis but "Normal" coronary angiography. Circulation 2001;104:2401-6.
26. Fearon WF, Luna J, Samady H et al. Fractional Flow Reserve Compared With Intravascular Ultrasound Guidance for Optimizing Stent Deployment. Circulation 2001;104:1917-22.
27. Kawamori H, Shite J, Shinke T et al. Natural consequence of post-intervention stent malapposition, thrombus, tissue prolapse, and dissection assessed by optical coherence tomography at mid-term follow-up. Eur Heart J Cardiovasc Imaging 2013;14:865-75.